SETAC PRESS

Environmental Toxicology and Chemistry, Vol. 30, No. 4, pp. 861–869, 2011

Printed in the USA
DOI: 10.1002/etc.445

IMPACT OF NANO TITANIUM DIOXIDE EXPOSURE ON CELLULAR STRUCTURE OF *ANABAENA VARIABILIS* AND EVIDENCE OF INTERNALIZATION

CARLA CHERCHI,† TATYANA CHERNENKO,‡ MAX DIEM,‡ and APRIL Z. GU*†
†Department of Civil and Environmental Engineering, Northeastern University, Boston, Massachusetts, USA
‡Department of Chemistry and Chemical Biology, Northeastern University, Boston, Massachusetts, USA

(*Submitted* 14 *July* 2010; *Returned for Revision* 6 *September* 2010; *Accepted* 5 *October* 2010)

Abstract—The present study investigated the impact of nano titanium dioxide ($nTiO_2$) exposure on the cellular structures of the nitrogen-fixing cyanobacteria *Anabaena variabilis*. Results of the present study showed that $nTiO_2$ exposure led to observable alteration in various intracellular structures and induced a series of recognized stress responses, including production of reactive oxygen species (ROS), appearance and increase in the abundance of membrane crystalline inclusions, membrane mucilage layer formation, opening of intrathylakoidal spaces, and internal plasma membrane disruption. The production of total ROS in *A. variabilis* cells increased with increasing $nTiO_2$ doses and exposure time, and the intracellular ROS contributed to only a small fraction (<10%) of the total ROS measured. The percentage of cells with loss of thylakoids and growth of membrane crystalline inclusions increased as the $nTiO_2$ dose and exposure time increased compared with controls, suggesting their possible roles in stress response to $nTiO_2$, as previously shown for metals. Algal cell surface morphology and mechanical properties were modified by $nTiO_2$ exposure, as indicated by the increase in cell surface roughness and shifts in cell spring constant determined by atomic force microscopy analysis. The change in cell surface structure and increase in the cellular turgor pressure likely resulted from the structural membrane damage mediated by the ROS production. Transmission electron microscopy (TEM) analysis of $nTiO_2$ aggregates size distribution seems to suggest possible disaggregation of $nTiO_2$ aggregates when in close contact with microbial cells, potentially as a result of biomolecules such as DNA excreted by organisms that may serve as a biodispersant. The present study also showed, for the first time, with both TEM and Raman imaging that internalization of $nTiO_2$ particles through multilayered membranes in algal cells is possible. Environ. Toxicol. Chem. 2011;30:861–869.

Keywords—Nanomaterials Ecotoxicity Algae *Anabaena variabilis* Nano titanium dioxide

INTRODUCTION

Progress in nanotechnology has raised concerns regarding the potential environmental impact of engineered nanomaterials (NMs). The increasing production rates of NMs and the utilization in various fields and commercial products are anticipated and will result in their release into aquatic habitats [1,2]. Particularly, titanium dioxide nanomaterials ($nTiO_2$) are being incorporated in a wide range of promising applications, which include solar energy conversion [3], cosmeceutical production [4], and biocidal processes, such as drinking water treatment for pathogen removal [5], because of their unique nano- and photocatalytic properties. Recently, detectable concentrations (5–15 μgTi/L) of titanium nanomaterials from wastewater treatment processes were revealed [6], in agreement with the predictions of Mueller and Nowack (0.7–16 μg/L) based on worldwide production volumes in typical Swiss environmental scenarios [7].

Currently, most nanotoxicity studies have focused on the cyto- and genotoxicology of $nTiO_2$ in human health initiated by exposure through the respiratory system, and the potential environmental implications of $nTiO_2$ for other organisms have largely been unexplored [1,8]. Fundamental research on the toxicity of $nTiO_2$ to ecologically relevant organisms, such as algae, bacteria, and fungi, is scarce [9]. The bioavailability and toxicity of $nTiO_2$ to algal ecosystems is of concern for the essential ecological role of prokaryotic and eukaryotic algae in primary productivity and aquatic food web chain equilibria [10]. A few studies have investigated the impact of NMs on algal ecosystems [11–13] using conventional regulatory toxicological methods with freshwater indicator microorganisms (*Selenastrum capricornutum, Desmodesmus subspicatus*) [3,14]. The results confirmed that exposure to $nTiO_2$ affects algal growth [3] and photosynthetic activity [12] and that abiotic parameters, such as particle size/aggregation and illumination, are key factors affecting $nTiO_2$ toxicity [15,16]. The underlying toxicity mechanisms of $nTiO_2$ nanomaterials have been elucidated to some extent, and they include membrane disruption [17], protein oxidation via reactive oxygen species (ROS) formation [9], and possible DNA damage [18]. Furthermore, persistence and bioaccumulation of $nTiO_2$ in cells is mostly unknown, and this potentially presents a concern for possible introduction into the food web.

Thus far, there has been no report on the ecotoxicity of NMs on cyanobacteria (also called blue-green algae), which are prokaryotes of significant biogeochemical importance because of their global contribution to nitrogen and carbon atmospheric fixation [10]. The abundance and unique metabolic strategies used by cyanobacteria to tolerate adverse and fluctuating conditions often make cyanobacteria good model algae for evaluating environmental stresses [19]. In the present study, we, for the first time, investigated the impact of $nTiO_2$ exposure on the cellular structures of the N-fixing cyanobacteria *Anabaena variabilis*. The effects on cell growth, intracellular structure, and cell surface properties were evaluated, and changes in cellular membranes, as well as cell surface topological and mechanical properties, were revealed. The oxidative stress caused by $nTiO_2$ by means of ROS production analysis was

All Supplemental Data may be found in the online version of this article.
* To whom correspondence may be addressed (april@coe.neu.edu).
Published online 23 December 2010 in Wiley Online Library (wileyonlinelibrary.com).

then quantified. The results provided a systematic evaluation of the $nTiO_2$ toxicity to the N-fixing cyanobacteria *Anabaena variabilis* and provided insights into the interreaction of $nTiO_2$ with algal cells.

MATERIALS AND METHODS

NMs preparation and characterization

Nano-TiO_2 anatase ($nTiO_2$; NanoStructured and Amorphous Materials) was prepared in culture Mes-Volvox medium in a stock concentration of 10 g/L, which contains 1% crude bovine serum albumin (BSA) as dispersant. An average size of NM aggregates of 192 ± 0.8 nm was determined through dynamic light scattering (Zetasizer Nano ZS90; Malvern Instruments) after nanomaterial dispersion in culture media (single crystal $nTiO_2$ primary size from manufacturer was 10 nm outer diameter). The stock solution was sonicated in a high-energy cup-sonicator (Fisher Scientific) at 90 W power for 20 min prior to tests. The polydisperisty index (PdI) after dispersion in culture media was found to be 0.479. A specific surface area (SSA) of $274.2\ m^2g^{-1}$ was previously reported for the $nTiO_2$ used in our study, by our collaborators Bello and colleagues [2]. Transition metals of the bulk material and other physical–chemical parameters (organic and elemental carbon, surface charge) determined for $nTiO_2$ suspension in phosphate-buffered saline were also reported by Bello et al. [2].

Culture conditions and ecotoxicological tests

Anabaena variabilis strain UTEX 1444 was axenically cultured at 20°C in a nitrogen-free modified Mes-Volvox medium containing 0.16 mM $MgSO_4 \cdot 7H_2O$, 0.16 mM Na_2-glycerophosphate $\cdot 5H_2O$, 0.67 mM KCl, 10 mM MES, 0.1 mM vitamin B_{12}, 0.1 mM biotin vitamin solution, and trace metals. Cells were cultured in 1-L chemostats with $0.15\ d^{-1}$ dilution rate, incubated under a 12:12-h light:dark regime using a 1:1 ratio of 34-W cool white and 40-W Sylvania gro-lux fluorescent bulbs. Chemostats were continuously mixed and aerated (air was filtered via 0.2-μm filtered compressed air at a rate of 5 ml/min), and algal concentration was maintained at 1.0 g/L of chlorophyll *a*. Cells from chemostats were used as starter for the stock culture preparation needed for toxicity tests. Aliquots (75 ml) of cultures with initial chlorophyll *a* concentration of 500 mg/L were subjected to different $nTiO_2$ concentrations (0–500 mg/L) and incubated for 96 h under the same conditions of culturing. Cells were periodically collected and prepared for various imaging analyses (atomic force microscopy [AFM], transmission electron microscopy [TEM], Raman; see below) to observe *A. variabilis* intracellular changes and $nTiO_2$ distribution.

Reactive oxygen species production: oxidative stress

Total ROS formation were determined according to the method described by Knuaert et al. [20] using the fluorogenic permeable probe 2′,7′-dichlorodihydrofluorescein diacetate (H_2DCFDA; Invitrogen). The probe is first hydrolyzed to the nonfluorescent dichlorodihydrofluorescein (H_2DCF) by cellular esterase before being transformed to the highly fluorescent dichlorofluorescein (DCF) in the presence of ROS and cellular peroxidases. Fluorescence associated with DCF was measured at certain time points using a Synergy™ HT Multi-Mode microplate reader (excitation filter 485 nm, emission filter 528 nm). Both total and intracellular ROS were analyzed with cells exposed to different concentrations of $nTiO_2$ (0–200 $mgTiO_2$/L) and different exposure times (0.5–2.5 h). To differentiate intracellular ROS from measured total ROS, cells were spin down by centrifugation (2,000 *g* for 10 min), replaced in fresh dye-free medium, and then subjected to fluorescence measurements. The DCF fluorescence results were expressed in terms of H_2O_2 units, because hydrogen peroxide (30%; Fisher Scientific) was used as a standard for ROS measurements.

Cell topology and mechanical properties changes

Anabaena variabilis cells exposed to 50 $mgTiO_2$/L for 24 h and those from controls without $nTiO_2$ exposure were dried by air onto the cleaved mica surfaces for cell surface characterization using AFM (Agilent 5500 Bio-AFM) analysis. Cell topography imaging and cell spring constant evaluation were obtained in contact mode at a low applied force of 0.2 N/m and scan rate of 1.04 s with rectangular nanoprobe cantilever of 0.05 N/m spring constant (k). Gwiddion 2.12 software (Gwyddion 2.12; General Public License, http://www.gwyddion.net, 2009) was used to analyze topographic images of cells. Cell surface roughness parameters (average roughness, Ra, and mean square roughness, Rq), for both *A. variabilis* cells exposed to $nTiO_2$ and those in control with no exposure were determined based on information obtained for a total of 20 random *A. variabilis* cells. For each cell, 25 ($300\ nm^2$) areas were selected at the center of the cell to avoid artifact resulting from edge effect to determine the average roughness and the root mean square roughness parameters. The cell spring constant (K_{cell}) was obtained from the slope of the linear portion of five deflection-piezo displacement curves determined per scanned cell, according to the method described by Francius et al. [21].

Intracellular modifications and spatial distribution of NMs

High-resolution TEM imaging was used to observe intracellular structural changes in *A. variabilis* as well as the spatial distribution and fate of NMs agglomerates. Cells were collected and fixed for 1.5 h at 4°C in Karnovsky's fixative. Specimens were then washed twice in 0.1 M cocodylate buffer and embedded in 2% agarose for beads preparations. Postfixation was completed in 2 h in 1% osmium tetroxide, followed by two rinsing steps in 0.1 M cocodylate buffer. A sequential dehydration series of beads in 30, 50, 70, 85, 95, and 100% ethanol was then followed by a gradual replacement of ethanol with Spurr's resin before completing infiltration and embedding in capsules. Capsules were placed in an oven and polymerized at 60°C for 24 h. Sample blocks were then trimmed and ultrathin sections (80 nm) obtained with a Diatome diamond knife with a Reichart Ultracut E Ultramicrotome. Ultrathin sections collected on 200 mesh copper grids were stained with 5% uranyl acetate and Reynold's lead citrate and observed with a JEOL JEM-1010 transmission electron microscope operated at 70 kV. Digital images were captured with an XR-41B bottom mount CCD camera system (AMT). Nanomaterial particles sizes were analyzed with the software Image J 1.43q (http://rsbweb.nih.gov/ij/).

Evaluation of $nTiO_2$ fate through Raman spectroscopy

In addition to TEM examination of NM presence, Raman microscopy was applied to identify and confirm the presence of $nTiO_2$ particles inside and/or outside the algal cells. Raman spectral images were acquired using a WITec model CRM 2000 confocal Raman microscope and a water-immersion objective ($\times 60/NA = 1.00$, working distance = 2.0 mm). Excitation ($\sim$30 mW at 488 nm) was provided by an air-cooled argon ion laser (Melles Griot). The exciting laser radiation was coupled to a Zeiss microscope through a wavelength-specific

single mode optical fiber. The backscattered light was finally detected by a back-illuminated deep depletion, 1,024- × 128-pixel charge-coupled device camera operating at −82°C. Three of the ten cells (exposed to 10 mg/L $nTiO_2$) analyzed via Raman microscopy showed intracellular presence of $nTiO_2$. Fixed samples were prepared on CaF_2 windows (Sigma-Aldrich) for imaging. The samples were placed on a piezoelectrically driven microscope scanning stage and raster scanned through the laser focus at 500-nm step size. Spectra were collected at a dwell time 250 msec. The Raman images presented have an overlay of color planes resulting from biomatrices and $nTiO_2$ spectral contributions, *x*,*y* resolution of approximately 3 nm and a repeatability of ±5 nm, and *z* resolution of approximately 0.3 nm and ±2 nm repeatability. The continuous motion prevents sample degradation at the focal point of the laser beam.

RESULTS AND DISCUSSION

Reactive oxygen species production after exposure to $nTiO_2$

The formation of ROS has been proposed as the primary mechanism inducing toxicity in cells exposed to $nTiO_2$ [22]. Once formed, ROS have the ability to activate a chain of radicals that can affect cellular components [17]. In the present study, oxidative status of *A. variabilis* cells exposed to different concentrations of $nTiO_2$ was monitored through the widely used and established DCFH-DA assay in order to determine intracellular (endogenous) and extracellular (exogenous) ROS. Results of the present study (Fig. 1a) showed a proportional production of ROS in *A. variabilis* cells with increasing $nTiO_2$ doses and exposure times under illuminating (growth) conditions. The increase in fluorescence of the dichlorofluorescein indicator over time measures the rate of total ROS production (Fig. 1b), and the ROS production rates increased from approximately 190 to 340 nM H_2O_2/h as the dose $nTiO_2$ concentrations increased from 10 to 200 mg/L. The intracellular ROS production determined at various $nTiO_2$ doses, as shown in Supplemental Data, Figure S1, contributed to only a small fraction (<10%) of the total ROS measured. Our results seem to be consistent with the study by Knauert and Knauer [20] on the green algae *P. subcapitata* exposed to Cu, in which they showed that more than 90% of the total ROS produced were found to be extracellular. These results indicate that either the primary toxic impact of $nTiO_2$ occurs at the membrane site, because the majority of ROS have been exogenously produced, or there might be transport of endogenous ROS (H_2O_2) to outside the cells, and the latter was reported through aquaporins in plants [20]. The dose-dependent ROS production confirms that $nTiO_2$ causes oxidative stress to *A. variabilis,* and the SoxRS regulatory machinery is recognized to play an important role in maintaining cellular viability, as previously indicated [18]. Although similar response mechanisms are characteristic of a broad spectrum of microorganisms, the production of ROS and the generation of hydroxyl radical have been found to be microbe dependent [23]; therefore, this result is specific to cyanobacteria and $nTiO_2$ interactions.

Intracellular modifications from $nTiO_2$ exposure

Analysis of the ultrathin TEM sections allowed the identification of modifications in *A. variabilis* subcellular structure when exposed to $nTiO_2$. The cross-section of a typical control cell of *A. variabilis* (vegetative cell) is shown in Figure 2a and clearly presents a typical radial arrangement of thylakoidal membranes, cellular sites of photosynthetic reactions, and various electron-dense or nondense intracellular inclusions of different functions (lipid inclusions, cyanophycin granules, etc). Under N-deficient conditions, vegetative cells develop heterocysts, specialized cells lacking photosystem II exhibiting structural and functional features distinct from those of vegetative-type cells. Figure 2e shows an untreated heterocyst with characteristic multicomponent envelope providing anoxygenic protection to the N-fixing activity of nitrogenase.

The structure of the cyanobacterium exhibited changes after exposure to various $nTiO_2$ concentrations and exposure times. The opening of intrathylakoidal spaces (Fig. 2b) and the appearance of intracellular open spaces was induced at all $nTiO_2$ concentrations tested (1, 50, 150 mg/L) and at different exposure times (24–96 h), with likely consequent alteration of the internal integrity of the cell. There was generally an increase in the percentage of cells with loss of thylakoids in the samples exposed to $nTiO_2$ compared with controls; however, a consistent dose-dependent trend was not found (Fig. 3). The reduction of these proteinaceous compartments might possibly indicate the loss of cellular photosynthetic potential and carbon fixation ability of *A. variabilis*, limiting the availability of important nutrients for growth, as previously indicated for *A. variabilis* cells exposed to Cd [24] or other heavy metals inducing stress conditions [25]. In a previous study [26], we observed that the

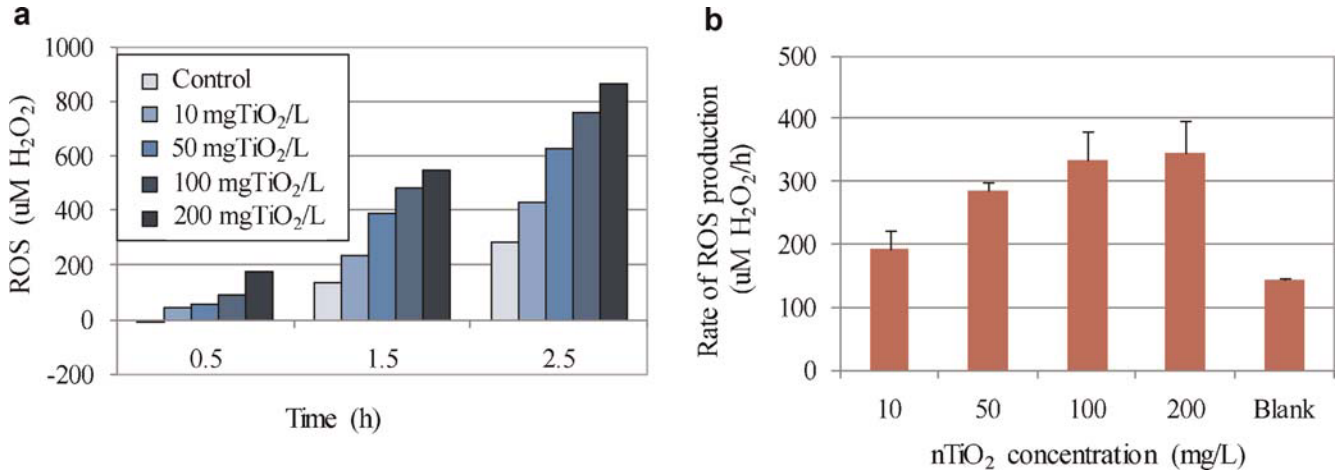

Fig. 1. Total reactive oxygen species (ROS) production (**a**) and total ROS production rate (**b**) in *Anabaena variabilis* samples exposed to $nTiO_2$ concentrations ranging from 0 to 200 mg/L for 2.5 h. [Color figure can be seen in the online version of this article, available at wileyonlinelibrary.com]

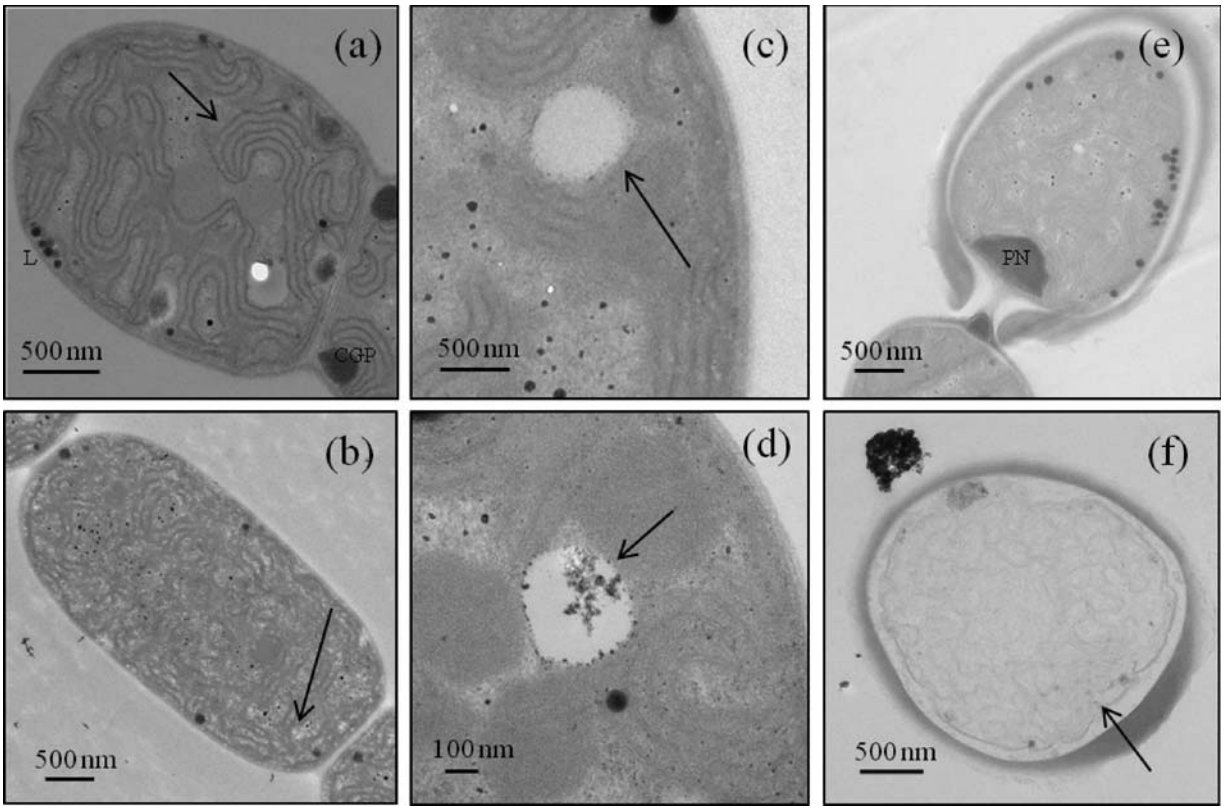

Fig. 2. Electron micrographs showing the effects of $nTiO_2$ exposure on *Anabaena variabilis* cells. *Anabaena variabilis* vegetative cell from control sample (**a**) with typical thylakoidal membranes (arrow), cyanophycin grana proteins, lipid inclusions (L). Opening of intrathylakoidal spaces in cell exposed to $nTiO_2$ (**b**). Membrane-limited inclusions without crystals in control sample (**c**) and with crystal in cell exposed for 48 h to 50 mgTiO_2/L (**d**). Typical heterocyst cell from control with polar nodule and thick envelope (**e**). Disruption of plasma membrane (arrow) in heterocyst after 24 h of exposure to 50 mgTiO_2/L (**f**).

growth and the N-fixation ability of *A. variabilis* was inhibited by $nTiO_2$ exposure with resulting median effective concentration 96 h (EC50-96 h) of 0.62 mg/L, and 0.4 mg/L, respectively. A possible imbalanced exchange or lack of nutrients between heterocysts and vegetative cell within the filament might have played a role in the toxicity effect.

The increase of crystals bound in intracellular membranes, also known as membrane-limited crystalline inclusions (Fig. 2c and d), was observed in cells exposed to various $nTiO_2$ concentrations and exposure durations. These inclusions exhibit a characteristic needle-like crystal structure that is usually found to be calcite, apatite, or hydroxyapatite [27]; their recognition is based on images from the literature and is facilitated by their characteristic morphology, shape, and location within the cells [27]. Compared with controls without any $nTiO_2$ exposure, there seemed to be an overall increase in the percentage of cells that showed crystalline inclusions. The relative abundance of cells with crystalline inclusions increased from 14% to as high as 27 to 57% in the samples exposed to $nTiO_2$ at various concentrations and exposure time lengths (Fig. 3). The functionality of these inclusions is largely unknown because of limited observations of this phenomenon. Previous investigations [28] showed an increase in the number of these crystals after exposure of *A. variabilis* and *Anabaena flos-aquae* to zinc, indicating its possible role in stress response to metals. Further studies on specific role and formation of these membranes structures during cellular stress response to $nTiO_2$ exposure are warranted.

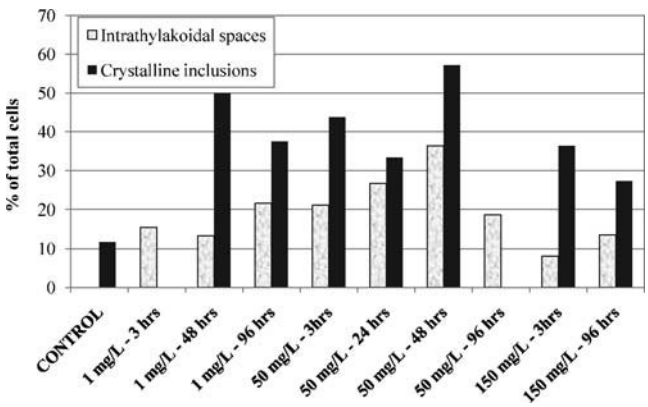

Fig. 3. Percentage of cells presenting intrathylakoidal spaces openings relative to the total cells observed and percentage of cells showing crystalline inclusions within the membrane-bound structure relative to the total cells scanned containing the membranes.

Disruption of internal plasma membranes in heterocyst cells was also observed and is shown in Figure 2f. Such a phenomenon was found to be common among cyanobacterial and algal cells under different types of stress conditions, such as the presence of allelochemicals [29] or the exposure to heavy metals [25].

Impact of $nTiO_2$ exposure

Structural and surface alterations induced in *A. variabilis* cells by the exposure of $nTiO_2$ were investigated and imaged via AFM. Several studies [30,31] have considered the AFM imaging technique as a suitable tool for investigating biological systems at high resolution and at the nanoscale level. Results of the present study indicated that cells surface topography and mechanical properties were modified after exposure to $nTiO_2$.

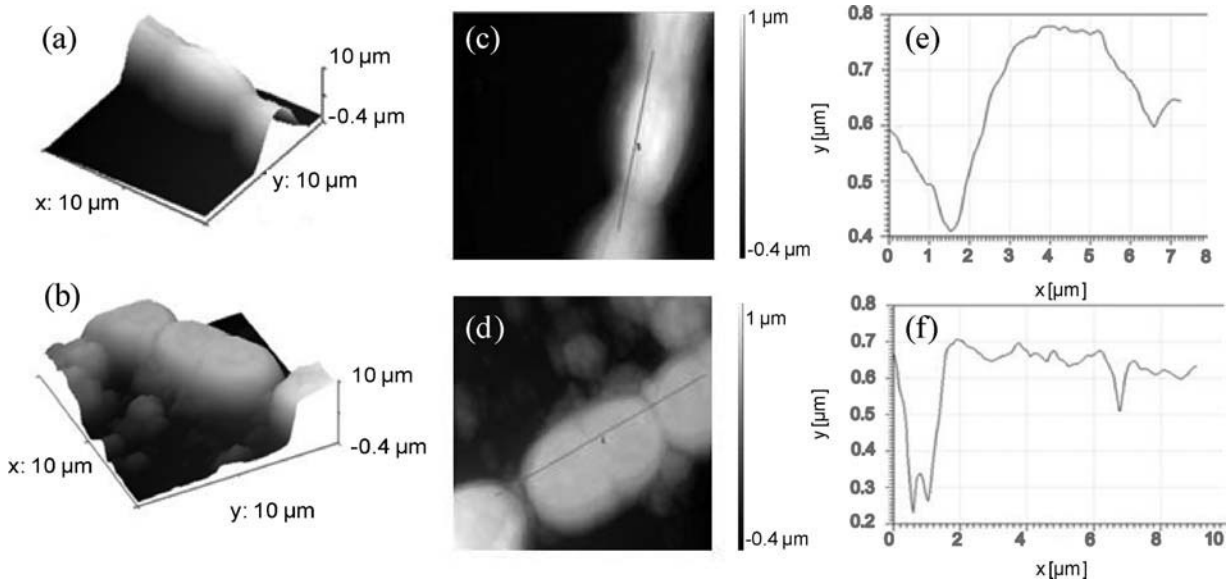

Fig. 4. Impact of $nTiO_2$ exposure on cell surface smoothness and topology. Comparison of atomic force microscopy results of control cell (top; **a, c, e**) and cell exposed to 50 mg/L of $nTiO_2$ for 24 h (bottom; **b, d, f**). Cell topographies (left; a, b), bidimensional image gray-graded by height with sections identified (middle; c, d) and section profiles (right; e, f).

Figure 4 shows representative AFM images to demonstrate the visual changes in cell surface topology (smoothness) after exposure to 50 mg/L for 24 h). As shown in Figure 4, the surface of unexposed cells (Fig. 4a, c, and e) appeared to be fairly smooth in comparison with those cells exposed to 50 mgTiO_2/L for 24 h (Fig. 4b, d, and f). Quantitative cell surface roughness analysis was conducted to confirm the changes in cell surface properties. Roughness values collected from 300-nm^2 areas of 20 untreated and exposed cells were fitted in log-normal distributions for comparison (Fig. 5a). The mean of roughness values (Ra) of exposed cells increased from 28.6 nm (measured in the control sample) to 45.9 nm, and the root mean square roughness parameter increased from 33.5 to 55.0 nm. Thus, the differences in roughness observed after the incubation of *A. variabilis* cells with $nTiO_2$ are possibly caused by morphological modifications at the cellular surface level or by $nTiO_2$ deposition onto cell membranes, as also shown previously in the TEM observations.

In the present study, AFM scanning also allowed us to probe the modifications occurring in the nanomechanical properties of *A. variabilis* cells after 24 h of exposure to 50 mg/L $nTiO_2$. To provide quantitative information on cellular surface mechanical properties, the bacterial spring constant (k_{cell}) was calculated based on the correlation between the force applied to the samples by the AFM cantilever and the indentation depth obtained. Arnoldi et al. [32] reported that the bacterial spring constant is a parameter directly related to the inner turgor pressure of the cell. The difference between the inner and the outer osmotic pressures required for preserving cellular shapes in cyanobacteria is typically 0.8 atm [32]. Our results showed that exposure to $nTiO_2$ caused changes in the cells spring constant (k_{cell}) distribution of native cells towards higher

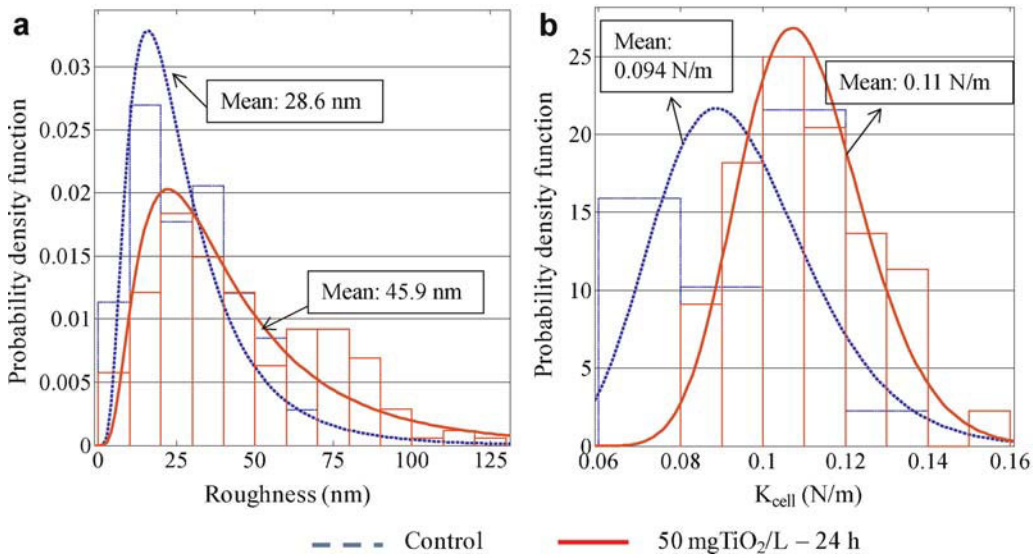

Fig. 5. Changes in the cell surface roughness (**a**) and in the cellular spring constant (**b**) as a result of exposure to 50 mgTiO_2/L for 24 h. The roughness data and cellular spring constant results were fitted in log-normal distributions and compared with the control. [Color figure can be seen in the online version of this article, available at wileyonlinelibrary.com]

x values (Fig. 5b). The mean of the log-normally fitted distribution of the spring constant (k_{cell}) increased from 0.094 N/m in untreated samples to 0.11 N/m after 24 h of exposure (at 50 mgTiO_2/L concentration). These values are in the range (0.01–0.5 N/m) of those reported in the existing literature and related to bacterial cells [31]. One possible explanation for the increase in cellular turgor pressure as a result of exposure to nTiO_2 can be inferred from a previous study by Cerf [33] based on heat-treated Gram-negative bacteria. Briefly, structural membrane changes may be explained by the mediation of ROS, which have the potential to modify protein structure [17], protein folding configuration, and periplasmic layer thickness at the cellular membrane level, which results in the collapse of membranes' layers. This generates an increase of water efflux in the membrane-folded compartments and, consequently, the increases in the contrasting cytoplasmic turgor pressure.

Impact on Anabaena variabilis *cellular membrane*

Disruption, alteration, and impairment of cellular membrane have been suggested as potential recognition mechanisms behind the antimicrobial activities exerted by NM exposure [17]. Transmission electron micrographs of cells exposed to different concentrations of nTiO_2 (1, 50, 150 mg/L) showed considerable changes in cell membranes upon treatment. Some of the *A. variabilis* cells observed (Supplemental Data, Fig. S2a and b) showed a lack of internal structural organization and compromised envelopes compared with the controls (Fig. 2a and e). Thus, vegetative and heterocyst cells were both damaged to a similar extent, revealing that heterocyst cells with functionally relevant thicker envelopes are also susceptible to lysis damage by nTiO_2. Freely released empty walls (data not shown) and intracellular material (Supplemental Data, Fig. S2c) from cell leakage or lysis was observed in exposed samples, likely related to the nTiO_2 potential to disrupt and oxidize the multilayered wall of *A. variabilis* cells. Membrane damage by nTiO_2 exposure likely occurs either through puncturing when direct cell–nanoparticle interaction occurs or perhaps via nTiO_2 adsorption onto cell surfaces (Supplemental Data, Fig. S2d and e). The main mechanism by which membranes are compromised may involve lipid peroxidation via ROS-mediated processes.

Prolonged (48–96 h) exposure of *A. variabilis* cells to nTiO_2 apparently has induced other cellular defense mechanisms, such as an increase in the outer mucilage layer thickness (Fig. 2f). This layer of protection, common in cyanobacteria, has not been found in the unexposed algal cells, but it was present in a few cells exposed for 96 h to 1 and 50 mgTiO_2/L with variable thickness ranging from 250 nm to 300 nm. Such phenomena have been found to be common among cyanobacterial and algal cells under different types of stress conditions (i.e., exposure to heavy metals [25]). A previous study by Reynolds [34] showed that the thickness and texture of the cyanobacterial mucilage are responsive to environmental variations, sequestration and storage of nutrients in deprived environments, exclusion of toxic metals, and general adaptation to conditions of stress. Our preliminary results demonstrated that an increase in outer mucilage layer thickness may be one of the nTiO_2-induced stress responses for *A. variabilis* as well; however, further studies are needed to confirm this phenomenon.

Evidence of internalization of nTiO_2 in algal cells

Literature on internalization of NMs by prokaryotic organisms is scarce, and it is thought that the possibility of transport of 100-nm-sized particles across 1-μm-sized prokaryotic cell membranes is likely only if the integrity of the cellular envelope has previously been compromised [17]. In the present study, we used combined Raman microscopy and TEM to observe the location and possible presence of nTiO_2 inside *A. variabilis* cells. Raman spectroscopy is a well-established method for the investigation of nanoparticle properties [35] as well as for the characterization of biological samples, such as algae [36]. High-resolution Raman images (Fig. 6) showed the spatial distribution of nTiO_2 inclusions inside individual cells in relation to the cellular organic matrix (C–H stretching region). Thus, simultaneous occurrence of Raman bands associated with nTiO_2 and C–H stretching demonstrates that the internalization of nanomaterials by *A. variabilis* cells is possible. nTiO_2-anatase appears with three major vibrations occurring at 400 cm^{-1}, 518 cm^{-1}, and 629 cm^{-1}, slightly shifted from the peaks identified by Robert and colleagues [37], most likely as a result of differences in NM particle size [35]. Major Raman peaks features at approximately 1,005 cm^{-1}, 1,155 cm^{-1}, and 1,525 cm^{-1} have also been highlighted in Figure 6c and are associated with carotenoids, typical pigments in algae. The most pronounced Raman intensity, between 2,800 and 3,050 cm^{-1}, originates from C–H stretching vibrations of the organic molecules of the organism. The confocal feature and the high Z-axis resolution of our Raman analysis confirmed that the nTiO_2 was indeed present inside *A. variabilis* cells, rather than possibly on top of or beneath the algal cells. To our knowledge, this is the first study showing the internalization of nTiO_2 by cyanobacteria algae cells, which is contrary to the previous hypothesis of inability of NMs to pass thick algal cell walls [13]. However, further studies are needed to understand fully the mechanisms involved in NMs transport through cell membranes at the nanoscale. It is not clear from the present study whether this NM internalization in the algal cells occurs after the cell damage or death via passive approach. At this stage, information is lacking on membrane pores' size in living cells and their real-time changes. Research has been oriented to establish the mechanisms of membrane transport, with a major focus on multidrug resistance and antibiotic treatments [38], but information is lacking on the mechanisms of NMs transport through cellular envelopes.

Insights into the impact of biomolecules on NMs aggregation

Time sequential TEM observations on algal cells exposed to different concentrations of nTiO_2 showed that, over the test period of 96 h, agglomeration of nTiO_2 (10-nm primary particles) occurred and resulted in various sizes of aggregates (115 aggregates observed across all samples tested), with an average longest dimension of 435.0 nm ± 275.5 nm (Supplemental Data, Fig. S3). Interestingly, the analysis of several TEM images showing NM aggregates surrounding algal cells seemed to suggest that NM aggregates could disrupt and release small NMs particles (10–20 nm) in very close proximity to algal cells (Supplemental Data, Fig. S3). Previous studies indicated that DNA [39] or other biomolecules released from cells may act as a dispersant and could facilitate the disaggregation of NM aggregates, which may explain what was observed here via TEM analysis. Previous literature showed the diffusion of 5-nm quantum dots through membranes of *Escherichia coli* and *Bacillus subtilis* [40], and nanosilver particles smaller than 80 nm were proven to pass through pores in membranes of living *Pseudomonas aeruginosa* cells [38]. The latter NM passing size was determined to be 50 times greater than the size of conventional detergent and antibiotic with proven capability to permeate cells envelopes [38]. Our finding implies that, although the NMs are expected to aggregate in media, the

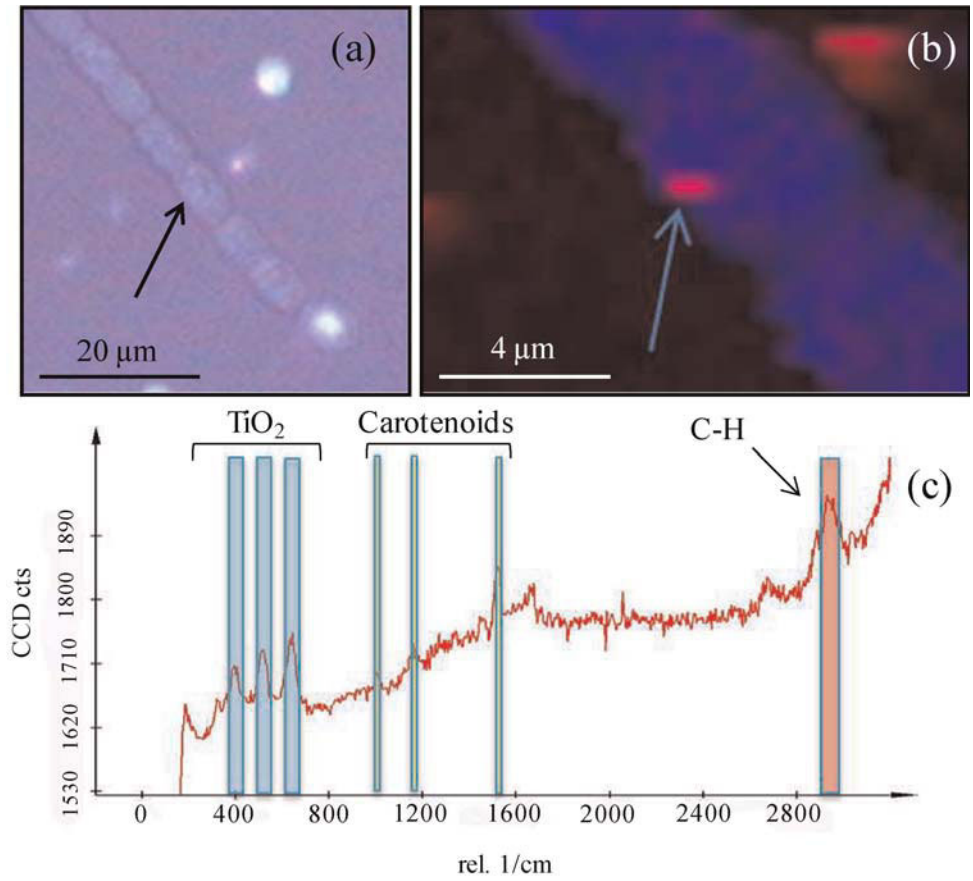

Fig. 6. High-resolution Raman images and Raman spectra of $nTiO_2$ internalization in *Anabaena variabilis* cells. Microscopic images taken with a water-immersion objective (×60; **a**), indicating a cell with inclusion (arrow). High-resolution images reconstructed from Raman intensities reflecting the protein density within the cell and the $nTiO_2$ inclusion (arrow; **b**). Spectra collected at the inclusion level showing characteristic $nTiO_2$ peaks (400 cm^{-1}, 518 cm^{-1}, and 629 cm^{-1}), carotenoids peaks (1,005 cm^{-1}, 1,155 cm^{-1}, and 1,525 cm^{-1}), and C–H stretching vibrations (2,800 cm^{-1} and 3,050 cm^{-1}). [Color figure can be seen in the online version of this article, available at wileyonlinelibrary.com]

primary single particle size for the NMs may be more important than the aggregates, because the latter is possibly dispersed by biomolecules excreted by organisms in the microenvironment when in close contact with microbial cells. This is consistent with the previous finding by Oberdörster [41], who found that the same-sized NM agglomerates originated from two different-sized $nTiO_2$ primary particles and exhibited different levels of toxicity.

CONCLUSIONS

The understanding of NMs interactions with algal ecosystems is still in its infancy, and the present study, for the first time, systematically investigated the impact of $nTiO_2$ on the N-fixing cyanobacteria *Anabaena variabilis*. The observed impact and cyanobacteria–$nTiO_2$ interactions are summarized in Table 1. Our results showed that $nTiO_2$ exposure led to

Table 1. Summary of impacts of $nTiO_2$ exposure on *Anabaena variabilis* morphology and intracellular structure observed at different $nTiO_2$ dosed concentrations and exposure durations

		$nTiO_2$ concentration and exposure time								
		1 mg/L			50 mg/L				150 mg/L	
	Impact of $nTiO_2$ on *Anabaena variabilis* morphology and intracellular structure	3 h	48 h	96 h	3 h	24 h	48 h	96 h	3 h	96 h
S[a]	Membrane disruption in vegetative and heterocysts cells				×	×	×	×	×	×
	Direct contact between $nTiO_2$ and cellular membranes		×	×	×	×	×	×	×	×
	Increase of membrane mucilage with variable depth		×	×				×		
I[b]	Internal plasma membrane disruption in heterocysts cells			×	×	×				
	Opening of intrathylakoidal spaces	×	×	×	×	×	×	×	×	×
	Release of intracellular material (biomolecules, etc.)				×					
	Appearance of membrane limited crystalline inclusions		×	×	×	×	×		×	×
S/I	Membrane roughness increase, morphological changes	×	×	×	×	×	×	×	×	×
	Modification of cellular mechanical properties					×				
	$nTiO_2$ diffusion through multilayered membrane			×				×		×

[a] Surface level.
[b] Intracellular level.

observable alteration in various intracellular structures and induced a series of recognized stress responses, including production of ROS, appearance of and increase in the abundance of membrane crystalline inclusions, membrane mucilage layer formation, opening of intrathylakoidal spaces, and internal plasma membrane disruption. Quantitative AFM analysis revealed that algal cells surface morphology and mechanical properties were modified, as indicated by the increase in cell surface roughness and shifts in cell spring constant upon $nTiO_2$ exposure. Our high-resolution sequential TEM image analysis seems to suggest possible disaggregation of $nTiO_2$ aggregates when in close contact with microbial cells, potentially as a result of biomolecules (e.g., DNA) excreted by organisms that may serve as biodispersant. The present study also showed evidence, for the first time, from both TEM and Raman imaging that the internalization of $nTiO_2$ particles through multilayered membranes in algal cells is possible; therefore, it may be transported along the ecological food web and ultimately impact important biogeochemical processes, such as the carbon and nitrogen cycle.

Acknowledgement—This work was supported by the National Science Foundation Nanoscale Science and Engineering Center (NSEC) for High-Rate Nanomanufacturing (NSF grant 0425826). We are grateful to Kai-tak Wan and his student Xin Wang (Northeastern University) for their assistance in the AFM analysis and to Dhimiter Bello and his student Anoop Pal (University of Massachusetts, Lowell) for DLS analysis. We are grateful to William Fowle from Northeastern University for his assistance with the TEM imaging.

SUPPLEMENTAL DATA

Figure S1. Intracellular reactive oxygen species (ROS) production in *Anabaena variabilis* cells exposed to various concentration of $nTiO_2$ ranging from 0 to 200 mg/L.

Figure S2. Electronmicrographs showing the effects of $nTiO_2$ exposure on *Anabaena variabilis* membranes in vegetative cell and heterocyst.

Figure S3. Transmission electron microscopy (TEM) images showing $nTiO_2$ aggregates and possible disaggregation in immediate adjacent area next to three distinct *Anabaena variabilis* cells exposed to 1 mgTiO_2/L and 50 mgTiO_2/L for 96 h. (630 KB PDF).

REFERENCES

1. Klaine SJ, Alvarez PJJ, Batley GE, Fernandes TF, Handy RD, Lyon DY, Mahendra S, McLaughlin MJ, Lead JR. 2008. Nanomaterials in the environment: Behavior, fate, bioavailability, and effects. *Environ Toxicol Chem* 27:1825–1851.
2. Rogers EJ, Hsieh SF, Organti N, Schmidt D, Bello D. 2009. Nanomaterials properties vs. biological oxidative damage: Implications for toxicity screening and exposure assessment. *Nanotoxicology* 3:249–261.
3. Aruoja V, Dubourguier HC, Kasemets K, Kahru A. 2009. Toxicity of nanoparticles of CuO, ZnO and TiO_2 to microalgae *Pseudokirchneriella subcapitata*. *Sci Total Environ* 407:1461–1468.
4. Nohynek GJ, Lademann J, Ribaud C, Roberts MS. 2007. Grey goo on the skin? Nanotechnology, cosmetic and sunscreen safety. *Crit Rev Toxicol* 37:251–277.
5. Theron J, Walker JA, Cloete TE. 2008. Nanotechnology and water treatment: Applications and emerging opportunities. *Crit Rev Microbiol* 34:43–69.
6. Kiser MA, Westerhoff P, Benn T, Wang Y, Perez-Rivera J, Hristovski K. 2009. Titanium nanomaterial removal and release from wastewater treatment plants. *Environ Sci Technol* 43:6757–6763.
7. Mueller NC, Nowack B. 2008. Exposure modeling of engineered nanoparticles in the environment. *Environ Sci Technol* 42:4447–4453.
8. Wang JJ, Sanderson BJS, Wang H. 2007. Cyto- and genotoxicity of ultrafine TiO_2 particles in cultured human lymphoblastoid cells. *Mutat Res Genet Toxicol Environ Mutagen* 628:99–106.
9. Neal AL. 2008. What can be inferred from bacterium-nanoparticle interactions about the potential consequences of environmental exposure to nanoparticles? *Ecotoxicology* 17:362–371.
10. Herrero A, Flores E. 2008. *The Cyanobacteria. Molecular Biology, Genetics and Evolution*. Caister Academic, Norfolk, United Kingdom.
11. Bouldin JL, Ingle TM, Sengupta A, Alexander R, Hannigan RE, Buchanan RA. 2008. Aqueous toxicity and food chain transfer of quantum Dots™ in freshwater algae and *Ceriodaphnia dubia*. *Environ Toxicol Chem* 27:1958–1963.
12. Navarro E, Piccapietra F, Wagner B, Marconi F, Kaegi R, Odzak N, Sigg L, Behra R. 2008. Toxicity of silver nanoparticles to *Chlamydomonas reinhardtii*. *Environ Sci Technol* 42:8959–8964.
13. Lin SJ, Bhattacharya P, Rajapakse NC, Brune DE, Ke PC. 2009. Effects of quantum dots adsorption on algal photosynthesis. *J Phys Chem C* 113:10962–10966.
14. Farre M, Gajda-Schrantz K, Kantiani L, Barcelo D. 2009. Ecotoxicity and analysis of nanomaterials in the aquatic environment. *Anal Bioanal Chem* 393:81–95.
15. Hund-Rinke K, Simon M. 2006. Ecotoxic effect of photocatalytic active nanoparticles TiO_2 on algae and daphnids. *Environ Sci Pollut Res* 13: 225–232.
16. Kahru A, Dbourguier HC, Blinova I, Ivask A, Kasemets K. 2008. Biotests and biosensors for ecotoxicology of metal oxide nanoparticles: A minireview. *Sensors* 8:5153–5170.
17. Wiesner MR, Bottero JY. 2007. *Environmental Nanotechnology. Applications and Impacts of Nanomaterials*. McGraw Hill, New York, NY, USA.
18. Kim S, Nishioka M, Hayashi S, Honda H, Kobayashi T, Taya M. 2005. The gene *ygg*E functions in restoring physiological defects of *Escherichia coli* cultivated under oxidative stress conditions. *Appl Environ Microbiol* 71:2762–2765.
19. Apte SK, Fernandes T, Badran H, Ballal A. 1998. Expression and possible role of stress-responsive proteins in *Anabaena*. *J Biosci* 23: 399–406.
20. Knauert S, Knauer K. 2008. The role of reactive oxygen species in copper toxicity to two freshwater green algae. *J Phycol* 44:311–319.
21. Francius G, Domenech O, Mingeot-Leclercq MP, Dufrene YF. 2008. Direct observation of *Staphylococcus aureus* cell wall digestion by lysostaphin. *J Bacteriol* 190:7904–7909.
22. Hirakawa K, Mori M, Yoshida M, Oikawa S, Kawanishi S. 2004. Photo-irradiated titanium dioxide catalyzes site specific DNA damage via generation of hydrogen peroxide. *Free Radic Res* 38:439–447.
23. Cho M, Chung HM, Choi WY, Yoon JY. 2005. Different inactivation behaviors of *MS-2 phage* and *Escherichia coli* in TiO_2 photocatalytic disinfection. *Appl Environ Microbiol* 71:270–275.
24. Rachlin JW, Jensen TE, Warkentine B. 1984. The toxicological response of the alga *Anabaena flos-aquae* (cyanophyceae) to cadmium. *J Archi Environ ContamToxicol* 13:143–151.
25. Surosz W, Palinska KA. 2005. Effects of heavy-metal stress on cyanobacterium *Anabaena flos-aquae*. *Arch Environ Contam Toxicol* 48:40–48.
26. Cherchi C, Gu AZ. 2010. Impact of titanium dioxide nanomaterials on nitrogen fixation rate and intracellular nitrogen storage in *Anabaena variabilis*. *Environ Sci Technol* 44:8302–8307.
27. Tamara B. 1993. *Ultrastructure of Microalgae*. CRC, New York, NY, USA.
28. Rachlin JW, Jensen TE, Warkentine B. 1985. Morphometric analysis of the response of *Anabaena flos-aquae* and *Anabaena variabilis* (Cyanophyceae) to selected concentrations of zinc. *J Arch Environ Contam Toxicol* 4:395–402.
29. Wu JT, Chiang YR, Huang WY, Jane WN. 2006. Cytotoxic effects of free fatty acids on phytoplankton algae and cyanobacteria. *Aquat Toxicol* 80:338–345.
30. Stoimenov PK, Klinger RL, Marchin GL, Klabunde KJ. 2002. Metal oxide nanoparticles as bactericidal agents. *Langmuir* 18:6679–6686.
31. Gaboriaud F, Dufrene YF. 2007. Atomic force microscopy of microbial cells: Application to nanomechanical properties, surface forces and molecular recognition forces. *Colloids Surfaces B Biointerfaces* 54: 10–19.
32. Arnoldi M, Fritz M, Bauerlein E, Radmacher M, Sackmann E, Boulbitch A. 2000. Bacterial turgor pressure can be measured by atomic force microscopy. *Phys Rev E* 62:1034–1044.
33. Cerf A, Cau JC, Vieu C, Dague E. 2009. Nanomechanical properties of dead or alive single-patterned bacteria. *Langmuir* 25:5731–5736.

34. Reynolds CS. 2007. Variability in the provision and function of mucilage in phytoplankton: facultative responses to the environment. *Hydrobiologia* 578:37–45.
35. Choi HC, Jung YM, Kim SB. 2005. Size effects in the Raman spectra of TiO_2 nanoparticles. *Vib Spectrosc* 37:33–38.
36. Marshall CP, Zhang Z, Coyle CM, Yilmaz K, Carter EA, Leuko S. 2006. Investigation of photosynthetic bacteria and algae by resonance Raman spectroscopy. *Proceedings*, 7th International Conference on Raman Spectroscopy Applied to Earth and Planetary Sciences, University of Valladolid, Valladolid, Spain, June 4-7, pp 97–98.
37. Robert TD, Laude LD, Geskin VM, Lazzaroni R, Gouttebaron R. 2003. Micro-Raman spectroscopy study of surface transformations induced by excimer laser irradiation of TiO_2. *Thin Solid Films* 440:268–277.
38. Xu XHN, Brownlow WJ, Kyriacou SV, Wan Q, Viola JJ. 2004. Real-time probing of membrane transport in living microbial cells using single nanoparticle optics and living cell imaging. *Biochemistry* 43:10400–10413.
39. Zheng M, Jagota A, Semke ED, Diner BA, Mclean RS, Lustig SR, Richardson RE, Tassi NG. 2003. DNA-assisted dispersion and separation of carbon nanotubes. *Nat Mater* 2:338–342.
40. Kloepfer JA, Mielke RE, Nadeau JL. 2005. Uptake of CdSe and CdSe/ZnS quantum dots into bacteria via purine-dependent mechanisms. *Appl Environ Microbiol* 71:2548–2557.
41. Oberdörster G. 2000. Toxicology of ultrafine particles: in vivo studies. *Philos Trans R Soc Lond A: Math, Phys, Eng Sci* 358:2719–2740.